Supplemental Document

Experimental simulation of time and frequency transfer via an optical satellite–ground link at 10^{-18} instability: supplement

QI SHEN,[1,2,3,†] JIAN-YU GUAN,[1,2,3,†] TING ZENG,[1,2,3] QI-MING LU,[1,2,3] LIANG HUANG,[1,2,3] YUAN CAO,[1,2,3] JIU-PENG CHEN,[1,2,3] TIAN-QI TAO,[2,4] JIN-CAI WU,[2,4] LEI HOU,[5] SHENG-KAI LIAO,[1,2,3] JI-GANG REN,[1,2,3] JUAN YIN,[1,2,3] JIAN-JUN JIA,[2,4] HAI-FENG JIANG,[1,2,3,5] CHENG-ZHI PENG,[1,2,3,6] QIANG ZHANG,[1,2,3,4,7] AND JIAN-WEI PAN[1,2,3,8]

[1]*Shanghai Branch, National Laboratory for Physical Sciences at Microscale and Department of Modern Physics, University of Science and Technology of China, Shanghai 201315, China*
[2]*CAS Center for Excellence and Synergetic Innovation Center in Quantum Information and Quantum Physics, University of Science and Technology of China, Shanghai 201315, China*
[3]*Shanghai Research Center for Quantum Sciences, Shanghai 201315, China*
[4]*Key Laboratory of Space Active Opto-Electronic Technology, Shanghai Institute of Technical Physics, Chinese Academy of Sciences, Shanghai 200083, China*
[5]*Key Laboratory of Time and Frequency Primary Standards, National Time Service Center, Chinese Academy of Sciences, Xi'an 710600, China*
[6]*e-mail: pcz@ustc.edu.cn*
[7]*e-mail: qiangzh@ustc.edu.cn*
[8]*e-mail: pan@ustc.edu.cn*
[†]*These authors contributed equally to this work.*

Supplement DOI: https://doi.org/10.6084/m9.figshare.14099291

Parent Article DOI: https://doi.org/10.1364/OPTICA.413114

Experimental simulation of time and frequency transfer via an optical satellite–ground link at 10^{-18} instability: supplemental document

This document provides supplementary information to "Experimental simulation of time and frequency transfer via an optical satellite–ground link at 10^{-18} instability". We present in detail the analysis for loss of the satellite-ground link, the experimental setup and parameters, the method of postprocessing, and some noise effect such as the amplifier and the atmosphere link.

1. SATELLITE GROUND LINK LOSS ANALYSIS

The main factors of transmission loss are full-angle divergence of the beam, the diameter of receiver's telescope, the optical effeciency of telescopes, and the transmittance of atmosphere. The whole equation can be written as Eq. S1.

$$\begin{aligned} \eta_{down} &= \eta_{tele\_s}(\frac{D_g}{L\theta_{down}})^2 T_{atm}\eta_{tele\_g}\eta_{sm\_g}, \\ \eta_{up} &= \eta_{tele\_g}(\frac{D_s}{L\theta_{up}})^2 T_{atm}\eta_{tele\_s}\eta_{sm\_s}, \end{aligned} \tag{S1}$$

where D_g and D_s are the telescope aperatures of ground and satellite, respectively, L is the satellite-to-ground distance. Supposing that the diameter for both telescopes is approximately 1 m, a typical dimension for optical space telescopes, θ_{down} and θ_{up} represent the effective transmitter full-angle divergence for the downlink and the uplink, respectively. It should be noted that the divergence angle not only includes the transmitter telescope divergence, but also the influence of atmospheric turbulence and the pointing error of the acquiring, pointing and tracking (APT) system. In transmission, the optical beam will be broadened or deflected by diffraction, air turbulence and mispointing, which are referred to here as diffraction loss. The diffraction loss of the uplink was $\left(\frac{D_s}{L\theta_{up}}\right)^2$, while for the downlink, this is $\left(\frac{D_g}{L\theta_{down}}\right)^2$. In the uplink, atmospheric turbulence close to the ground strongly deteriorates the quality of the beam. Therefore, turbulence-induced distortion will significantly increase the beam divergence angle. The divergence angle is about 22 μrad according to our previous result related to the 'Micius' satellite [1]. The atmospheric seeing in observatory stations is commonly smaller than 10 μrad. With the adaptive optics system, the effects of turbulence can be partially compensated for [2]. The pointing error of the APT system will lead to spot position jitter, which also influences the effective divergence angle. This effect can be smaller for satellite in higher orbits due to the smaller angular velocity and acceleration than with satellites in low orbits. Thus, it is reasonable to obtain 15 μrad of θ_{up} with a comparatively large transmitter telescope aperture and optimized adaptive optics. In the downlink, the beam reaches the air turbulence with a large size and is received immediately after crossing the atmosphere, thus, the impact of air is much smaller for the beam broadening compared to that of the uplink, meaning the effective divergence angle can be close to the diffraction limit. With the optical wavelength of 1550 nm and the diameter of telescope on satellite 1 m, the divergence angel of 4 μrad for θ_{down} is technically achievable [3].

The telescope optical efficiency of satellite and ground are η_{tele_s} and η_{tele_g}, respectively, both of which were set to 0.8. Given the two-way link symmetry, the satellite telescope was the transmitter for the downlink and the reciever for the uplink. T_{atm} is the atmosphere transmittance, which is reduced by the air absorption and the scattering of the propagating beam. The attendant value is related to the visibility, the altitude and the optical wavelength, etc., with the typical value around 0.7 for 1,550 nm at a sea-level location with 5-km visibility[4]. Meanwhile, η_{sm_s} and η_{sm_g} represent the single-mode fiber coupling efficiency on the satellite and on the ground, respectively. In terms of the ground, for the downlink, the adaptive optics technology could be employed to optimize the coupling efficiency to over 15% [5], while for the uplink, since the receiver was in a

Satellite	LEO		MEO		GEO	
Height(km)	1,000		10,000		36,000	
Link	Downlink	Uplink	Downlink	Uplink	Downlink	Uplink
Total loss (dB)	23.8	40	43.8	60	54.9	71.1
Radial velocity (km/s)	≈ 6		≈ 1		≈ 0.001	
Passage time (s)	$\approx 10^3$		$\approx 10^4$		$\approx 10^6$	
Point-ahead angle (μrad)	45.9		29.8		17.3	

Table S1. The estimation of link loss, radial velocity, passage time and point-ahead angle for each type of satellites. The loss becomes higher according to orbit altitude, while the radial velocity becomes smaller. The Doppler effect is proportional to the radial velocity. The divergence angle is 4 μrad and 15 μrad for downlink and uplink, respectively. The single-mode fiber coupling efficiency is 15% and 5% for downlink and uplink, respectively. The aperture of the receive telescope is 1 m and the telescope efficiency is 80%, for both satellite and ground.

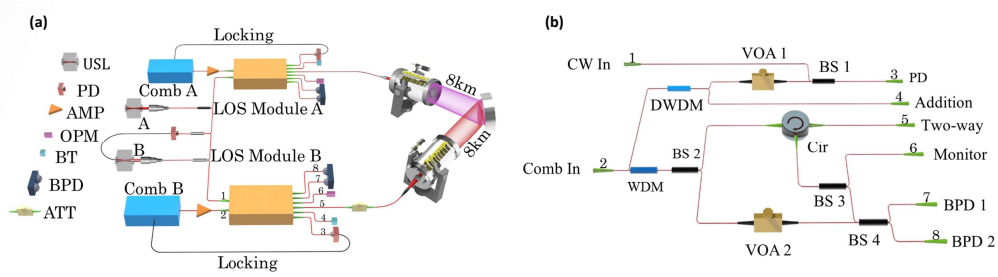

Fig. S1. (a). Our experimental setup. USL: Ultra-stable laser. PD: Photo diode. AMP: Amplifer. BT: Beam trap. ATT: Attenuator. OPM: Optical power meter. BPD: Balanced photon diode. LOS Module: a compact box for linear optical sampling; (b) the detailed structure in our LOS Module. WDM: A 20-nm band-pass filter centered at 1,520 nm. DWDM: A 0.8-nm narrow filter centered at 1,550.12 nm. Cir: Circulator. VOA 1 and VOA 2: Attenuator. BS 1: 50:50 beam splitter for beat between CW laser and comb. BS 2: 99:1 beam splitter, its 99% port is connected to the circulator. BS 3: 95:5 beam splitter, its 5% port is connected to the monitor port. BS 4: 50:50 beam splitter for beat between local comb and signal.

high-speed moving satellite and the single-mode fiber receiving field of view was very small, the single-mode coupling efficiency was very sensitive to the optical axis consistency between the ground and the satellite telescope. This was estimated to be 0.05 for uplink. The comparison of the links for each type of satellite is shown in Table S1.The satellite orbit is assumed to be circular with a zero-degree inclination. The ground station is set in the equator line and the field of view is 150° from the minimum elevation angle of 15°. The radial velocity is calculated with the satellite at the elevation angle of 15° from the horizon plane of the ground station.

2. EXPERIMENTAL SETUP AND PARAMETERS

In our experiment, terminal A and B each has a optical frequency comb (OFC) and an ultra-stable laser. The ultra-stable laser act as a frequency reference or a clock. The OFC is used to transfer the phase of the ultra-stable laser to time, and is further used in linear optical sampling (LOS) to extract the time difference of two combs. The whole setup is shown in Fig. S1a. To estimate the performance of time and frequency transfer itself, one ultra-stable lasers is syntonized to another. The phase difference of two syntonized lasers should always be zero at the locking point, which it is the beam splitter between two ultra-stable lasers in Fig. S1a. This is the reference plane in our experiment. The actual time offset given by LOS reflect the noise of the whole link, thus implies the stability of the time and frequency transfer setup.

The repetition rate of terminal A's comb was defined as 250 MHz, that is, we split the repetition frequency by a factor of 25 and used it as the 10 MHz reference clock for all our electrical systems.

Meanwhile, the repetition frequency of terminal B's comb was 2.6 kHz higher than that of terminal A. We used a 20-nm band-pass filter centered at 1,520 nm to filter out the part with the highest intensity in the comb's spectrum. The band was lower than the Nyquist frequency of LOS to ensure the LOS did not produce any aliasing. The reflected light of the filter then passed through a 0.8-nm narrow filter centered at 1,550.12 nm and beat with the 1,550.12-nm ultra-stable laser. The linewidth of the ultra-stable laser was sub-Hz and the stability was 3×10^{-15} at 1 second.

To compensate for the large link loss, we had to minimize the local optic loss with some consideration of the limited laser power. The detailed structure of this module is shown in Fig. S1b. First, we noted that the intensity for the local oscillator of LOS only required around 200 μW, meaning the ratio of first beam splitter (BS) after the 20-nm band-pass filter was 99:1. Almost the whole of the comb's beam went to the two-way port. Then, to split the forward signal and backward signal, a circulator was used. Due to a certain amount of insertion loss with fiber components, we determined the forward loss of the box from the comb input port to the two-way port to be 2.5 dB and the backward loss of the box from the two-way port to the beam splitter for LOS to be 3 dB. This value of loss could be further suppressed if we use all free space optics to minimize the coupling loss in future work.

According to the papers [6, 7] of the NIST group, their output power of the frequency comb at the transmit aperture is around 2.5 mW and the average value of received power is 33 nW, corresponding to a total channel loss of below 50 dB. For our case, the output power of frequency comb at the transmit aperture is around 120 mW (Note that 250 mW power in total but around 3 dB loss with the optical components and fibers in the sending side) and the average received power is about 10 nW, corresponding a channel loss of 72 dB (Calculating from 171 mW at two-way port of LOS module at sending side). To overcome such a big extra-loss, we improve the optical coupling efficiency of 6 dB by circulation manipulation (as shown in Fig. S2) and bear 6 dB lower received optical power, resulting in a low signal to noise ratio and more bad data, in additional to increasing the laser power by using an EDFA. The circulator is exploited to replace beam splitter (BS) for combining the input comb and local comb, which saves 3 dB each. The circulator setup will bring in longer non-reciprocal path, which brings more noise. This problem is solved by carefully adjust the length of each path and pack it in a small box. After temperature stabilization using thermo-electric coolers (TEC), no influence to the stability is seen at E-19 level in the system floor test.

The performance of our home-made balanced detector is similar to that of NIST. The necessary received power is about 6 nW in our local test, corresponding to 187 photons/pulse. The standard deviation for a single measurement is about 60 fs. However, with lower received optical power (6 dB) and lager power fluctuation due to a longer air path, we push the system to a more critical and more realistic experimental condition to simulate a space link. To improve the sensitivity, one need to suppress the background noise, and a narrow band-pass filter may be used. The drawback is that the filter limits the Doppler shift of the optical frequency, thus limits the maximum velocity the system can tolerate. In our setup, only a 100 MHz low-pass filter is used, and in principle we can tolerate velocity up to $\pm$ 75 m/s. This is enough for a GEO satellite.

The power of the comb had to be further improved to tolerate the high loss of the uplink of the GEO satellite. An additional comb amplifier with a two-level amplification was thus employed in our experimental setup to test the frequency transfer with a 72-dB link. The final output power was 250 mW in a 20-nm band. The band-pass filter is inputed in the amplifier so we replaced the 20-nm band-pass filter in the LOS module with a 98:2 beam splitter. The forward loss of the new LOS module is reduced to 1.7 dB. The power at the two-way port of the LOS module was 171 mW. The average received power is about 10 nW, and the average loss between two LOS module is 72.4 dB.

In our system, the reference frequency was determined via the stable laser at terminal A. We can write the relationship of frequency as $f_{laser,A} = f_{CEO,A} + M * f_{rep,A} + f_{beat,A}$, where $f_{laser,A}$ is the frequency of the stable laser, $f_{CEO,A}$ is the CEO frequency, $f_{rep,A}$ is the repetition frequency, and the $f_{beat,A}$ the beat frequency between the comb teeth and the stable laser. Because the stable laser was the only clock in our system, the repetition rate of the comb should only be determined according to the frequency of the stable laser. That is, a small drift of carrier-envelope offset (CEO) frequency must not influence the repetition rate. To achieve this goal, the ideal method involves using self-referencing, which lock the both $f_{CEO,A}$ and $f_{beat,A}$ to a frequency proportion to $f_{rep,A}$. Here, we used an easier method that required no modification in terms of the default configuration of the frequency comb. The frequency comb uses an internal rubidium clock as a reference clock for all its electrics. We set the CEO frequency and the beat frequency to the

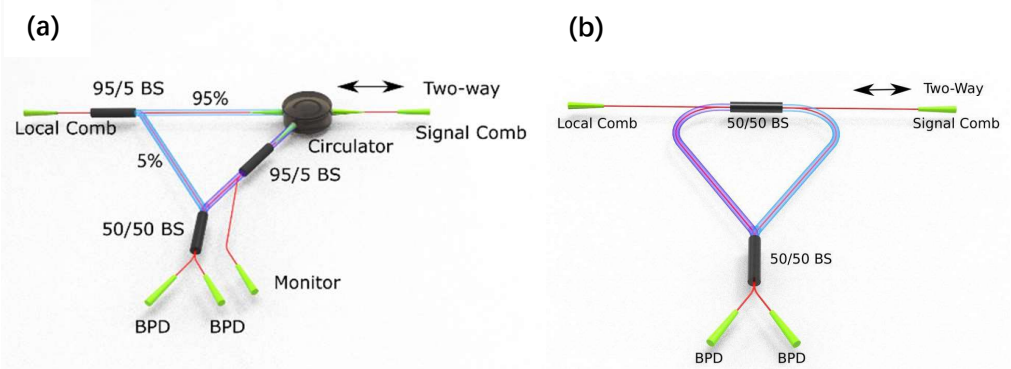

Fig. S2. Comparison of the lineal optical sampling optical setup between our setup and NIST setup. (a). In this work, the splitting ratio of BS2 is 99:1, thus almost all beam goes to Two-way port. The return signal from the Two-way port passed a circulator and most of them arrived at balanced photon diodes. (b). In the NIST work [6, 7], both 3 dB loss is included for forward and backward directions because of the 50:50 beam splitter. So total optical coupling efficiency of 6 dB is saved with circulation manipulation.

same value and adjusted their sign to make $f_{CEO,A} = -f_{beat,A}$. Thus, we had $f_{laser,A} = M * f_{rep,A}$, which means the repetition frequency of the comb was only related to the optical frequency of the stable laser. The same approach was then used on terminal B.

After locking the comb to the stable lasers, the two lasers at each side had to be syntonized such that they represented the same clock. Here, the "same clock" does not mean that the difference between the absolute frequency of the two lasers was always fixed; rather, it means that the frequency of the second laser was always proportional to the frequency of the first. When terminal A's stable laser had a drift of 10 kHz, terminal B's stable laser had to have a corresponding shift, albeit not exactly 10 kHz. The simplest solution here was to beat the two ultra-stable lasers, and locking the beat frequency to a local oscillator which is syntonized with the repetition rate of terminal A's comb. Because $f_{laser,A} = M * f_{rep,A}$, we had $f_{laser,B} - f_{laser,A} \propto f_{rep,A} \propto f_{laser,A}$, meaning the two stable lasers could achieve syntonization.

Dispersion compensaten is another point in our experiment. The linear optical sampling works best for two transform-limited pulse or for two pulse with exactly same dispersion theoretically. Actually, to optimize the linear optical sampling the dispersion is not entirely canceled in our system, and the received pulse width is about 4 ps. We use non-zero dispersion-shifted fiber (NZDSF) to compensate part of the dispersion. When the length of NZDSF is too short, the dispersion widens the interferogram and reduces the SNR. However, too long NZDSF fiber will induce much non-linear effect, the interferogram is deformed and also worsen the system performance. We also tried dispersion compensation fiber (DCF), but the splicing loss is high because of the different fiber core diameter. This will reduce the maximum tolerated loss of our system. From another point of view, the dispersion in real satellite-ground link is vary with the pitch angle of the satellite, thus limits the pulse width without a difficult real-time compensating. The atmosphere dispersion may vary in the order of 0.1 ps^2 estimated from the Ciddor Equation [8]. For our combs with 2-THz bandwidth, the minimum pulse width is limited to 1-2 ps. Thus we think the 4 ps pulse duration in our experiment is enough to mimic the real satellite-ground time transfer.

3. LOS AND TIME OFFSET EXTRACTION

One way to extract the high-precision time is through LOS, which required that the two optical combs had a slight difference in terms of repetition rate. When they beat with each other, the pulse from one comb slowly stepped by another, generating a series of inteference points with difference voltages. We refer to these points as a 'frame'. The interference signals then had to go through a low-pass filter and could thus be recorded for further analysis. To clearly show how to extract the time offset, it is useful to analyze it within the frequency domain. We can write the

electric field of the two combs as follows:

$$E_A(t) = \exp(i2\pi\omega_A t)\sum_n [E_{A,n}\exp(i2\pi n f_r t)]\,, \tag{S2}$$

$$E_B(t) = \exp(i2\pi\omega_B t)\sum_n [E_{B,n}\exp\left(i2\pi n(f_r+\Delta f_r)t\right)]\,. \tag{S3}$$

Here, ω_A and ω_B are the optical frequencies of one pair of most adjacent teeth of two combs. The difference between ω_A and ω_B is smaller than $f_{rep,A}/2$. The repetition frequency of terminal A's comb was f_r, while terminal B's comb had a slightly higher repetition frequency of $f_r + \Delta f_r$. After the low-pass filter with bandwidth $f_r/2$, only the beat of most of the adjacent frequencies was maintained. Thus the voltage was as follows:

$$\begin{aligned} V(t) \propto & \mathrm{Im}\left[E_A^*(t)E_B(t)\right] = \mathrm{Im}[\exp[i2\pi(\omega_B-\omega_A)t] \\ & \times\sum_n E_{A,n}^* E_{B,n}\exp[2i\pi n\Delta f_r t]]. \end{aligned} \tag{S4}$$

Now, supposing that terminal B's comb had a delay τ, note that $\tau \in [-\frac{1}{2f_r}, \frac{1}{2f_r})$, otherwise, we could align the pulse of terminal A's comb to another pulse of terminal B's. This delay resulted in the interferogram experiencing a temporal shift, and the corresponding phase of the frequency spectrum underwent a change in slope. We can write the new interferogram as follows:

$$\begin{aligned} V(t,\tau) \propto & \mathrm{Im}\left[E_A^*(t)E_B(t-\tau)\right] = \mathrm{Im}[\exp\{i2\pi[(\omega_B-\omega_A)t-\omega_B\tau]\} \\ & \times\sum_n E_{A,n}^* E_{B,n}\exp[2i\pi(n\Delta f_r t - n(f_r+\Delta f_r)\tau)]]. \end{aligned} \tag{S5}$$

We use $S(\nu,\tau)$ to represent the Fourier transform of the interferogram. Here ν is the frequency obtained from the FFT of the interferogram, τ is the delay of the link. $S(\nu,\tau)$ is the spectral value at FFT frequency ν and $\angle S(\nu,\tau)$ represents the spectral phase. From equations S4 and S5, we have,

$$\begin{aligned} &\angle S(\nu,0) = 0 \\ &\angle S(\nu,\tau) = -2\pi\tau\frac{f_r+\Delta f_r}{\Delta f_r}[\nu-(\omega_B-\omega_A)] - 2\pi\omega_B\tau. \end{aligned} \tag{S6}$$

The phase is a linear function to ν, and the slope of frequency spectrum $-2\pi\tau\frac{f_r+\Delta f_r}{\Delta f_r}$ is proportional to the delay τ. It is worth noting that the phase $\angle S(\nu,\tau)$ has no relation with spectrum shape $E_{A,n}, E_{B,n}$. The low-frequency amplitude noise and spectrum-related noise such as Gordon-Haus jitter has a negligible contribution to τ.

After the calculation of the precise delay τ, the clock offset Δt can be easily derived through the principle of two-way time synchronization: $T_{A\to B} = T_{Link} - \Delta t$, $T_{B\to A} = T_{Link} + \Delta t$. The atmosphere usually suffers low-frequency noise such as wind and turbulence, meaning T_{Link} is stable during a ten-millisecond period. Thus, we have,

$$\Delta t = \frac{1}{2}(T_{B\to A} - T_{A\to B}). \tag{S7}$$

The linear optical sampling requires a fixed frequency difference for the two combs. From Eq. S6, it is clear that the slope is inversely proportional to the Δf_r. Given a specific interferogram, the delay time τ is proportional to the pre-set value of Δf_r. An incorrect value of Δf_r can lead to a continuous drift of τ, and this will soon exceed the ambiguous range of $\frac{1}{f_r}$. Thus, a real frequency transfer using LOS must be used to calibrate the frequency difference. Here, because our two stable lasers were locked with each other, we could obtain the frequency difference through a simple calculation. At first, we have $f_{laser,A} = M * f_{rep,A}$ and $f_{laser,B} = N * f_{rep,B}$. Using a wavelength meter that is accurate to 10 MHz, the value of M and N can be precisely determined. Because the $f_{rep,A} = 250$ MHz, the $f_{laser,A}$ can be calculated. Then, we get the value of $f_{rep,B}$ and $f_{laser,B}$. The parameters are listed in Table S2.

After calculating the Δf_r, we had to extract the time offset and track its change. For our frequency transfer experiment, we ignored the initial time offset of the two clocks, only focusing on the relative change in time offset. Thus, for each frame, we only extracted the time offset relative to the first frame, which involved two processes. During the first process, we carried

$f_{rep,A}$	250 MHz
M	773,603
$f_{laser,A}$	193.400,75 THz
$f_{rep,B}$	250.002,600,8 MHz
N	773,592
$f_{laser,B}$	193.400,011,96 THz
Δf_r	2,600.802,5 Hz

Table S2. The parameters of our experiment. The frequency reference is the repetition rate of terminal A's comb, which means $f_{rep,A}$ is defined as 250 MHz.

out FFT analysis on the frame data to obtain the phase information. Then we calculated the phase difference between this frame and the first frame. The slope and the time offset τ could then be determined. In this step, the influence of system dispersion was also canceled out. For the second process, we calculated the time offset value for an ideal clock at that specific frame. More specifically, because the interval of the adjacent pulse for the two combs was different, for every pulse of terminal A's comb, the corresponding pulse of terminal B's comb would go a bit quicker. The difference was $dt = \frac{\Delta f_r}{f_r(f_r+\Delta f_r)}$. Given the start position for the first frame and this frame, named p_1 and p_N, in the unit of the interval of terminal A's comb, we know that the theoretical time offset provided by terminal B's comb was always accurate. The value was $\tau_{theo} = \mathrm{mod}((p_N - p_1) \times dt, \frac{1}{f_r})$. Thus, we had to subtract this from the value of τ. In other words, the value of $\tau = \tau_{theo}$ as calculated in the first process, actually means the time offset was not changed.

The interferogram in our experiment updates every 380 μs, which is exactly $\frac{1}{\Delta f_r}$. For simplicity, we used one acquisition card with two channels to record both terminal A's and terminal B's interferograms. Limited by the transmitted speed from the acquisition card to the computer, we only recorded about 10 frames every second. Then we extracted 1024 samples from the middle of each interferogram. Further algorithms including Fast Fourier Transform (FFT), phase unwrapping, and linear fitting algorithms, provided the final time offset τ.

Finally, it is important to pay some attention to the sign of the time offset. We can recall that only one acquisition card was used to record two LOS signals. The LOS at terminal A meant the arrived time of terminal B's signal had a delay equal to T_{Link}, which gives a negative slope, while at terminal B's side, the arrived time of terminal A's signal had a delay equal to T_{Link}, which was equivalent to that of the arrived time of terminal B's signal T_{Link} ahead. The LOS at terminal B's side now finally presents a positive slope. Thus, we should flip the sign of τ at terminal B's side. Finally, the formula $\Delta t = \frac{1}{2}(T_{B\to A} - T_{A\to B})$ provided the correct change in time offset during the whole experiment.

In our experiment, to tolerate loss as large as possible, the hardware trigger threshold of the acquisition card is set with a quite low level. This will also introduce many noise. That is, not all interferograms are 'correct' interferograms. The most spikes is actually caused by the incorrect data. To filter these noise, we first get the angle difference between each interferogram and the first one. The angle should have a linear relation with the FFT frequency in principle. The slope is calculated by the least square method. The final time offset is proportional to the slope. At the same time, we can estimate the confidence interval of the slope using statistical theory. The noise interferograms often give a poor linear fitting, thus results in a large confidence interval. By setting a threshold for the confidence interval, almost all noise interferograms are removed. More than 91% of the original data is retained. Note that we hadn't use any assumptions or knowledge about the clocks of the two places until this step. After that, there is still a few spikes in the phase data. We removes the phase spikes larger than 500 fs. These points corresponding to frequency jump larger than at least 400 Hz in our data, which is impossible for two ultra-stable lasers with a 3×10^{-15} stabiltiy. As long as the stability of the two clocks can be effectively estimated, we can forecast the range of frequency difference and remove large spike points.

After all the post-processing steps, we got the final data of clock offset. The clock offset in 72-dB link experiment is shown in Fig. S3. We then calculate the corresponding time deviation (TDEV)

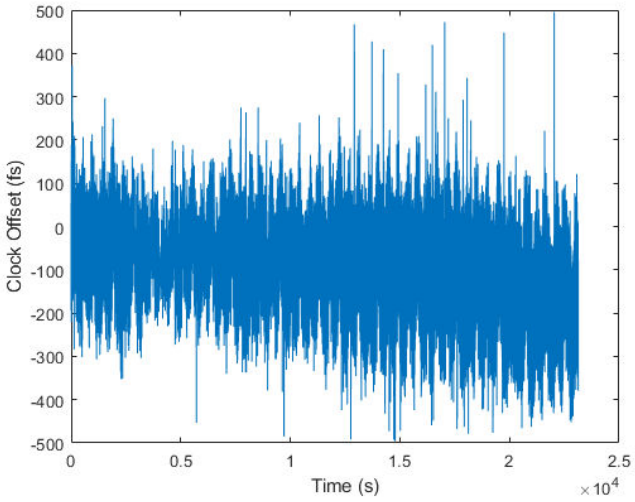

Fig. S3. The measured clock time offset data.

from the clock offset data and show it in Fig. S4. The modified Allan deviation (MDEV) data in main text is calculated from TDEV using formula $M_{DEV} = \frac{\sqrt{3}T_{DEV}}{\tau}$.

4. NON-LINEAR EFFECT OF AMPLIFICATION

The high optical power can induce possible non-linear effect, including additional frequency and intensity noise to the comb and spectrum variation. Although, we believe that the nonlinear effect can be neglect, we should address in the text. First, the additional frequency or phase noise due to amplification is suppressed by the phase locked loop; the modified allan deviation of the in-loop optical beat signal between the amplified optical frequency comb (OFC) and the stable laser is measured to be 2E-16 with 1 second average, which is well below the air link, as shown in Fig. S5. Therefore, we can conclude that the additional phase noise effect is negligible.

Second, we have observed that the relative amplitude noise of the amplified OFC signal is a few orders lower than that of the received power, as shown in Fig. S6. Then, additional intensity noise due to amplification is not dominated effect. The relative intensity noise (RIN) of the amplified laser is also shown in Fig. S7, the intensity noise degenerates a little,but still maintains low noise level.

Finally, we add the spectrum information, as shown in Fig. S8, and find that the spectrum of valid wavelength is much more stable than the received optical power. Because the variation of the spectrum can convert to an equivalent power variation, so we believe that the spectrum change does not dominate this experiment. Especially, we have measured the noise floor which contains all noise effect except for the air path, as shown in Fig. S9. It can be seen that the noise floor of time-frequency transfer with amplification is almost the same as that without amplification. So the influence of the non-linear effect of 250 mW amplification on the performance of time-frequency transfer can be negligible.

In order to tolerate higher channel loss, one direct way is to increase the optical power of the frequency comb. High optical power can induce possible non-linear effect, including additional frequency and intensity noise to the comb and spectrum variation. In our setup, the nonlinear effect of 250 mW amplification can be neglect. A higher power, however, may induce larger nonlinear effects, which will increase the equivalent attenuation of the link, and reduce the performance of the LOS. It would be useful to study how to minimize the nonlinear effect at even higher powers.

5. CHARACTERIZATION OF THE FREE SPACE LINK

This experiment is carried out through a horizontal density air-path with a distance of 16 km in a noisy city, which is well-beyond the effective thickness of the aerosphere, which is typically

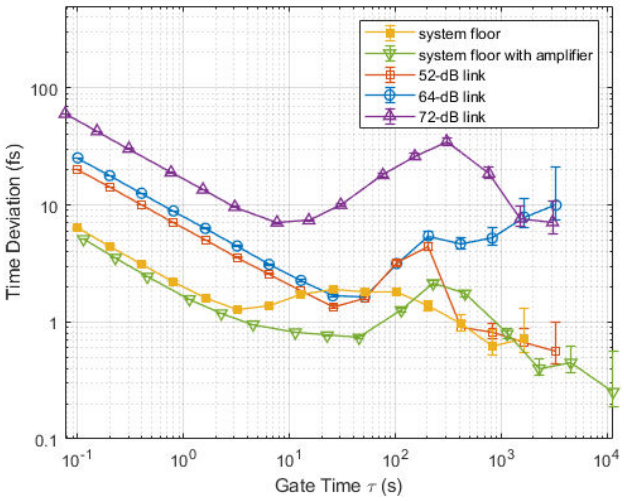

Fig. S4. Calculated TDEV of time-frequency transfer.

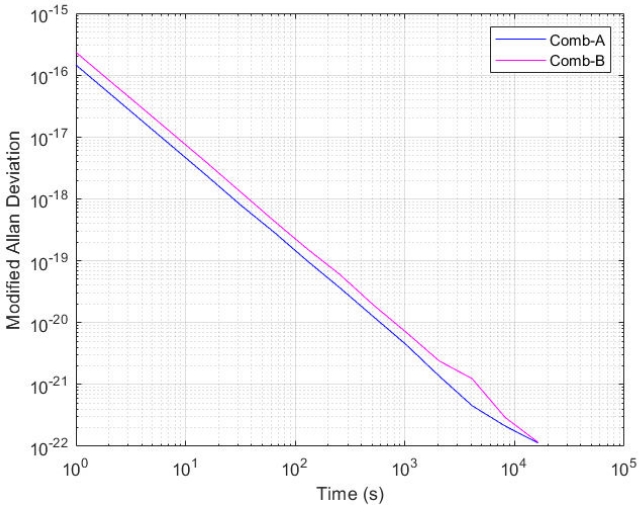

Fig. S5. The modified allan deviation of the in-loop optical beat signal between the amplified optical frequency comb (OFC) and the stable laser.

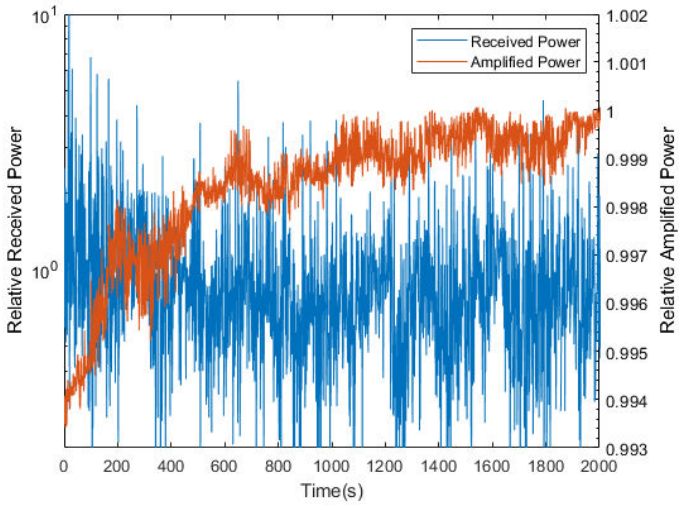

Fig. S6. The relative amplitude fluctuation of the amplified OFC signal and the received power after 16 km free space atmosphere link.

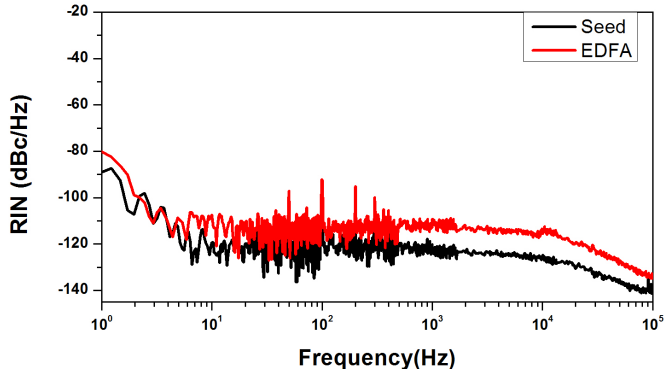

Fig. S7. The relative intensity noise (RIN) of the amplified laser. Seed represents the frequency comb power of about 5 mW into the amplification. EDFA represents the 250 mW output comb power.

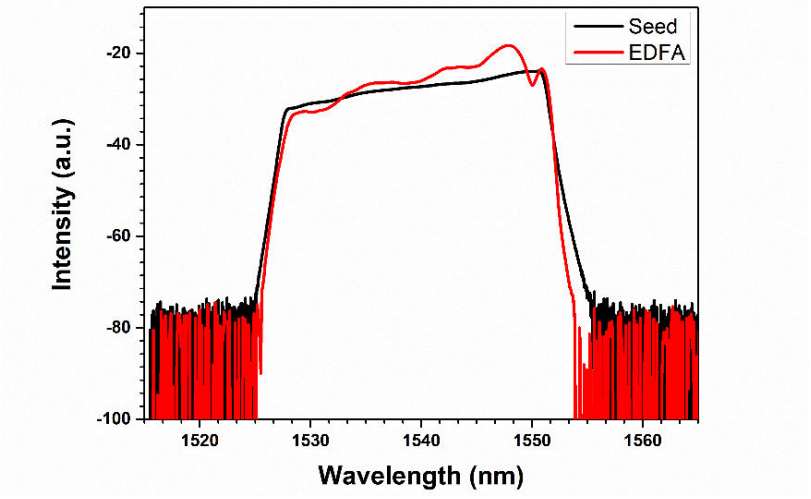

Fig. S8. The spectrum distribution of the OFC at the position before and after the EDFA.

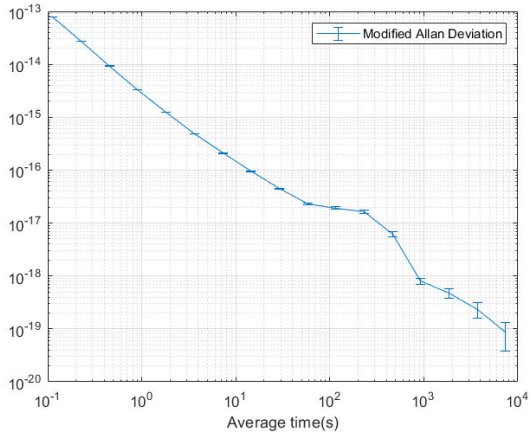

Fig. S9. The noise floor of the time-frequency transfer setup which contains all noise effect of the 250 mW amplification except for the air path.

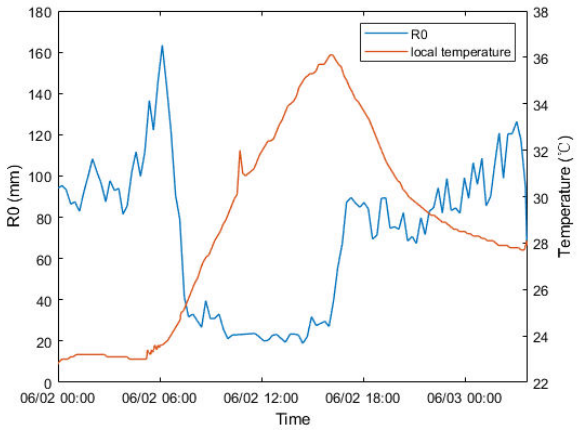

Fig. S10. The typically measured Fried's parameter of our ground atmosphere link of one way 8 km distance as well as the environment temperature.

below 10 km [9]. Actually, the measured atmospheric turbulence over one way length of 8 km show that the turbulence effect is greater than that of a satellite-to-ground link. The typically measured Fried's parameter [10] of our ground atmosphere link is between 2 cm to 16 cm (shown in Fig. S10), while typical values for Fried's parameter of satellite-to-ground link range from 10 cm for average seeing to 20 cm under excellent seeing conditions for a typical astronomical optical observatory [11]. Fluctuations of the recieved power extending below the detection threshold result in a signal "dropout" and no timing information been obtain. The dropout time is calculated by making the difference between adjacent data and the histogram is shown below in Fig. S11. 90% of the dropouts are below 130 ms. The typical measured Fried's parameter (R0) of the ground 8 km atmosphere link is range from 6 cm to 10 cm. The variation in the one-way relative link time-of-flight delay is also given in Fig. S12. The maximum one-way time delay drifts to around 17 ps during about 20,000 s period.

The link quality has a direct impact on short-term stability. On the one hand, the loss of the link determined the received power, thus affect the measurement precision. We have done some tests about the relationship between measurement precision and received power [12]. On the other hand, the poor link often leads to frequent dropout, decreases the data sample rate. In our experiment, the 52-dB and 64-dB links should have higher count rate than the 72-dB link. However, due to the transmittion speed of the hardware, the acquisition speed for the 52-dB and 64-dB links is limited to an average value of 10 Hz. We then use the data of the 72-dB link to show the influence of the count rate on the short-term stability. We split the raw data into groups every 1000 seconds. Then we calculate the count rate and MDEV at 1 second. The relationship between

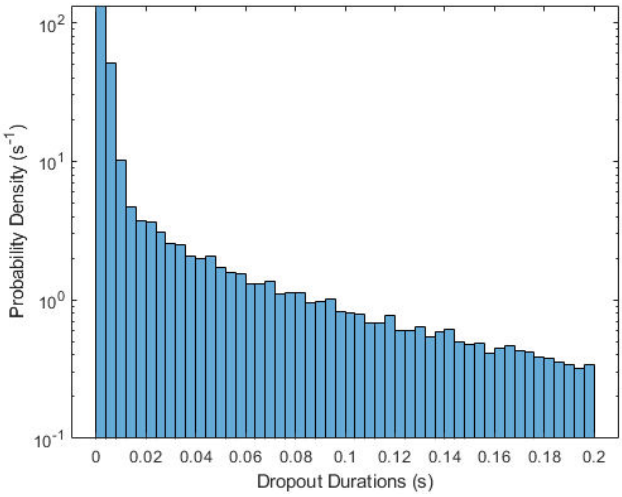

Fig. S11. Probability density of dropouts of the link versus duration.

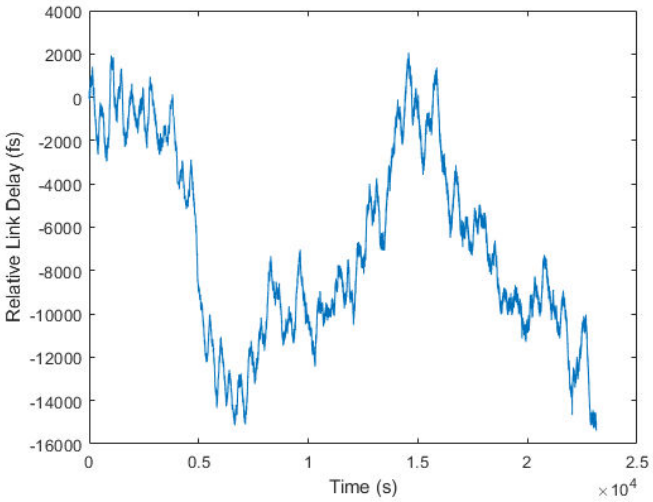

Fig. S12. The variation in the one-way relative link time-of-flight delay.

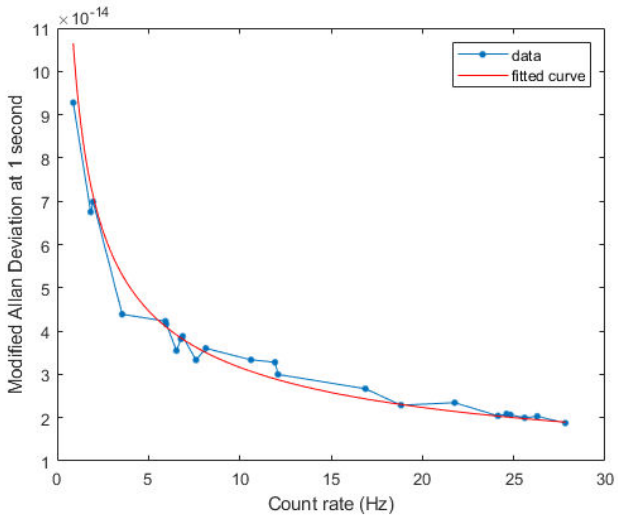

Fig. S13. The relationship between MDEV at 1 second and the count rate. The theoretical $1/\sqrt{N}$ curve fits well.

the two quantities is shown in Fig. S13. And Fig. S14 shows that the count rate dominates the short-term stability with three typical subsets of data.

REFERENCES

1. J.-G. Ren, P. Xu, H.-L. Yong, L. Zhang, S.-K. Liao, J. Yin, W.-Y. Liu, W.-Q. Cai, M. Yang, L. Li *et al.*, "Ground-to-satellite quantum teleportation," Nature **549**, 70 (2017).
2. D. Vasylyev, A. A. Semenov, and W. Vogel, "Atmospheric quantum channels with weak and strong turbulence," Physical Review Letters **117**, 090501 (2016).
3. Y. Cao, Y.-H. Li, W.-J. Zou, Z.-P. Li, Q. Shen, S.-K. Liao, J.-G. Ren, J. Yin, Y.-A. Chen, C.-Z. Peng, and J.-W. Pan, "Bell Test over Extremely High-Loss Channels: Towards Distributing Entangled Photon Pairs between Earth and the Moon," Physical Review Letters **120**, 140405 (2018).
4. J. Bourgoin, E. Meyer-Scott, B. L. Higgins, B. Helou, C. Erven, H. Huebel, B. Kumar, D. Hudson, I. D'Souza, R. Girard *et al.*, "A comprehensive design and performance analysis of low earth orbit satellite quantum communication," New Journal of Physics **15**, 023006 (2013).
5. N. Jovanovic, N. Cvetojevic, C. Schwab, B. Norris, J. Lozi, S. Gross, C. Betters, G. Singh, O. Guyon, F. Martinache *et al.*, "Efficiently feeding single-mode fiber photonic spectrographs with an extreme adaptive optics system: on-sky characterization and preliminary spectroscopy," in "Ground-based and Airborne Instrumentation for Astronomy VI," , vol. 9908 (International Society for Optics and Photonics, 2016), vol. 9908, p. 99080R.
6. J.-D. Deschênes, L. C. Sinclair, F. R. Giorgetta, W. C. Swann, E. Baumann, H. Bergeron, M. Cermak, I. Coddington, and N. R. Newbury, "Synchronization of distant optical clocks at the femtosecond level," Physical Review X **6**, 021016 (2016).
7. F. R. Giorgetta, W. C. Swann, L. C. Sinclair, E. Baumann, I. Coddington, and N. R. Newbury, "Optical two-way time and frequency transfer over free space," Nature Photonics **7**, 434 (2013).
8. P. E. Ciddor, "Refractive index of air: new equations for the visible and near infrared," Appl. Opt. **35**, 1566–1573 (1996).
9. C.-Z. Peng, T. Yang, X.-H. Bao, J. Zhang, X.-M. Jin, F.-Y. Feng, B. Yang, J. Yang, J. Yin, Q. Zhang, N. Li, B.-L. Tian, and J.-W. Pan, "Experimental free-space distribution of entangled photon pairs over 13 km: Towards satellite-based global quantum communication," Phys. Rev. Lett. **94**, 150501 (2005).
10. L. C. Andrews, *Field guide to atmospheric optics* (SPIE Press, 2004).
11. J. S. Lawrence, M. C. B. Ashley, A. Tokovinin, and T. Travouillon, "Exceptional astronomical seeing conditions above Dome C in Antarctica," Nature **431**, 278–281 (2004).
12. Q. Lu, Q. Shen, J. Guan, M. Li, J. Chen, S. Liao, Q. Zhang, and C. Peng, "Sensitive linear

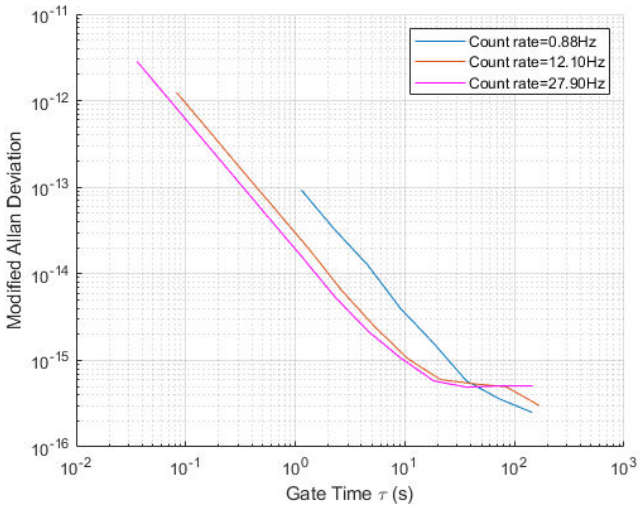

Fig. S14. The MDEV of three typical subsets of data with different count rate. The subsets of data is chosen from the experimental data of 72-dB link, each has a duration of 1000 seconds. The count rate for each dataset is 0.88 Hz, 12.1 Hz and 27.9 Hz.

optical sampling system with femtosecond precision," Review of Scientific Instruments **91**, 035113 (2020).